Table X. Comparison of Ratios of Magnetic Moments to Ratios of Squares of Isotropic *g* Values for Isoelectronic Transition-Metal Complexes

metal	μ(bds)/μ(bdt)	$[\langle g\rangle$(bds)/$\langle g\rangle$(bdt)$]^2$
Co	1.049	1.045
Ni	1.060	1.053

4.3 (±0.5) Å. The significance of this observation lies in the fact that the unpaired electron density cannot be primarily on the transition-metal atom (i.e., the Co) alone or distributed over the entire complex, including the organic ligands, but rather primarily distributed over the transition metal and the four chalcogen atoms.

The **g** tensors, which are summarized in Table IX, show that the electronic ground states of the cobalt complexes do not arise from orbitally degenerate states (i.e., from states possessing E-type symmetry) because the **g** tensors are orthorhombic.

(d) General Observations. The magnetic moment varies as the square of the isotropic *g* value. Thus, it is of interest to compare the ratios of the magnetic moments of isoelectronic pairs of complexes (e.g., $Ni(bds)_2^-$ and $Ni(bdt)_2^-$)[4] with the ratio of the square of their respective isotropic *g* values taken from Tables VI and IX. The results are shown in Table X. The agreement is quite good.

ESR studies and the static magnetic susceptibility data on $Co(bds)_2^-$ and $Ni(bds)_2^-$ clearly indicate that there is no cooperative magnetic interaction between paramagnetic spin sites in either complex (i.e., each spin state acts independently of all of its neighbors). This is consistent with the observed crystal structure of these complexes, in which each magnetic entity is physically rather far from its nearest neighbor.

Registry No. 3, 87143-01-9; **1b**, 107658-47-9; $(n\text{-}C_4H_9)_4N^+Ni(bds)_2^-$, 96030-04-5; $(n\text{-}C_4H_9)_4N^+Co(bds)_2^-$, 96030-06-7; $(n\text{-}C_4H_9)_4N^+Cu(bds)_2^-$, 96042-48-7; $(n\text{-}Bu)_4N^+Ni(bdt)_2^-$, 15077-51-7; $(n\text{-}Bu)_4N^+Co(bdt)_2^-$, 15186-37-5; $(o\text{-}C_6H_4Se)_x$, 107658-48-0; *o*-dibromobenzene, 583-53-9; sodium diselenide, 39775-49-0; thiophosgene, 463-71-8.

Supplementary Material Available: Tables SI–SIII, listing thermal parameters, nonessential bond lengths and angles, and least-squares planes, and a figure showing the geometry and labeling scheme for the tetrabutylammonium ion (4 pages); a table of observed and calculated structure factors (6 pages). Ordering information is given on any current masthead page.

Contribution from the Department of Chemistry, University of Virginia, Charlottesville, Virginia 22901, AT&T Bell Labs, Murray Hill, New Jersey 07974, and Bell Communications Research, Murray Hill, New Jersey 07974

Extended X-ray Absorption Fine Structure (EXAFS) Studies of a Soluble Chevrel Phase

D. A. Holtman,[1a] B. K. Teo,*[1b] J. M. Tarascon,[1c] and B. A. Averill*[1a,d]

Received April 7, 1986

The structure of the one-dimensional chains within $Li_2Mo_6Se_6$ in propylene carbonate solution was investigated by means of extended X-ray absorption fine structure (EXAFS) spectroscopy and compared to that of the crystalline $M_2Mo_6Se_6$ (M = Li, In, Tl) phases. The Fourier-transformed Mo K-edge EXAFS displays three peaks at r' = 2.4, 3.5, and 4.2 Å (r' = distance uncorrected for phase shift), while the Fourier-transformed Se K-edge EXAFS exhibits four peaks at r' = 2.3, 3.5, 4.3, and 4.9 Å. The Mo EXAFS was modeled with a theoretical single-electron single-scattering EXAFS equation using a total of five backscattering pairs, and the Se EXAFS was fit with a total of six backscattering pairs. The similarity of the solution- and solid-phase EXAFS spectra of $Li_2Mo_6Se_6$ indicates that the bulk of the Mo and Se atoms in solution experience an environment indistinguishable from that within the solid phase; this is consistent with retention of, essentially, unaltered $(Mo_3Se_3^-)_\infty^1$ strands in solution.

Polynuclear Mo^{II}–Y (Y = S, Se) clusters have been the object of much study in recent years, with most attention focused on the Chevrel phases ($Mo_6Y_8^{n-}$, n = 0, 2) because of their intriguing superconductivity properties.[2] In the search for novel superconductors in the Mo^{II}–chalcogenide system, new clusters formed by the linear confacial condensation of discrete Mo_6 octahedra were discovered.[3] These cluster compounds are often difficult to characterize, both physically and structurally, due to their amorphous nature and insolubility. EXAFS has proved useful in initially characterizing the most recalcitrant of these compounds. EXAFS characterization of the one-dimensional chains observed in $M_2Mo_6Se_6$ solid phases and its recently reported solution phase[4] was initiated to assess structural modifications within the chains resulting from interchain interactions and crystal-packing forces. Transmission electron microscopy (TEM) results[4] suggest that in 10^{-3}–10^{-4} M solutions the linear chains of $(Mo_3Se_3^-)_\infty^1$ form bundles that are roughly 20 Å in diameter and 10 μm in length. We report herein the first Mo and Se K-edge EXAFS of the solubilized phase and its comparison with the EXAFS of the corresponding solid phases of the one-dimensional chains within $M_2Mo_6Se_6$ (M = Li, In, Tl). Because of the large number of coordination shells within 5 Å of the source atom and the large number of components of each coordination shell, the EXAFS of the extended cluster compounds proved difficult to analyze. The demonstration that the spectra are tractable to analysis and an examination of *intra-* and *inter*chain interactions in the crystalline and solution phases is of importance to an understanding of these low-dimensional materials.

Experimental Section

Samples of solid $Tl_2Mo_6Se_6$, $In_2Mo_6Se_6$, and $Li_2Mo_6Se_6$ and solutions of $Li_2Mo_6Se_6$ dissolved in propylene carbonate ($Li_2Mo_6Se_6$/PC; ca. 0.01 *m*) were prepared as described.[5] The samples are air-stable except for $Li_2Mo_6Se_6$ and its solutions, which were handled under an N_2 atmosphere. Mo and Se K-edge (19.999 and 12.652 keV, respectively) absorption spectra were recorded in transmission mode at room temperature at the Cornell High Energy Synchrotron Source (CHESS). The K-edge absorption spectra of $Li_2Mo_6Se_6$ and $Li_2Mo_6Se_6$/PC, which are typical for the compounds studied, are shown in Figures 1 and 2.

The data reduction procedure for the compounds studied here is similar to that reported previously by us.[6-8] The EXAFS analysis utilized

(1) (a) University of Virginia. (b) AT&T Bell Labs. Current address: Department of Chemistry, University of Illinois at Chicago, Box 4348, Chicago, IL 60680. (c) Bell Communications Research. (d) Alfred P. Sloan Fellow, 1981–1985.

(2) Matthias, B. T.; Marezio, M.; Corenzwit, E.; Cooper, A. S.; Barz, N. E. *Science (Washington, D.C.)* **1972**, *175*, 1465. Fischer, O.; Odermatt, R.; Bongi, G.; Jones, N.; Chevrel, R.; Sergent, M. *Phys. Lett. A* **1973**, *45A*, 87. Fischer, O.; Treyvaud, A.; Chevrel, R.; Sergent, M. *Solid State Commun.* **1975**, *17*, 721.

(3) (a) Potel, M.; Chevrel, R.; Sergent, M. *Acta Crystallogr. Sect. B: Struct. Crystallogr. Cryst. Chem.* **1980**, *B36*, 1545. (b) Potel, M.; Chevrel, R.; Sergent, M.; Decroux, M.; Fischer, O. *Acta Crystallogr. Sect. B: Struct. Crystallogr. Cryst. Chem.* **1980**, *B36*, 1319. (c) Gougeon, P.; Pena, O.; Potel, M.; Sergent, M.; Brusetti, R. *Ann. Chim. (Paris)* **1985**, *9*, 1079.

(4) Tarascon, J. M.; DiSalvo, F. J.; Chen, C. H.; Carroll, P. J.; Walsh, M.; Rupp, L. *J. Solid State Chem.* **1985**, *58*, 290.

(5) Tarascon, J. M.; Hull, G. W.; DiSalvo, F. J. *Mater. Res. Bull.* **1984**, *19*, 915.

(6) Teo, B. K. *Acc. Chem. Res.* **1980**, *13*, 417.

0020-1669/87/1326-1669$01.50/0

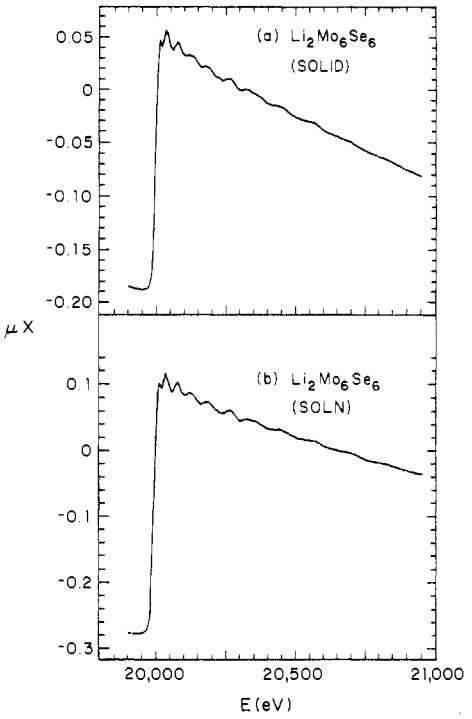

Figure 1. Mo K-edge of (a) $Li_2Mo_6Se_6$ and (b) $Li_2Mo_6Se_6$/PC displayed as ln (A/A_0) vs. E in eV.

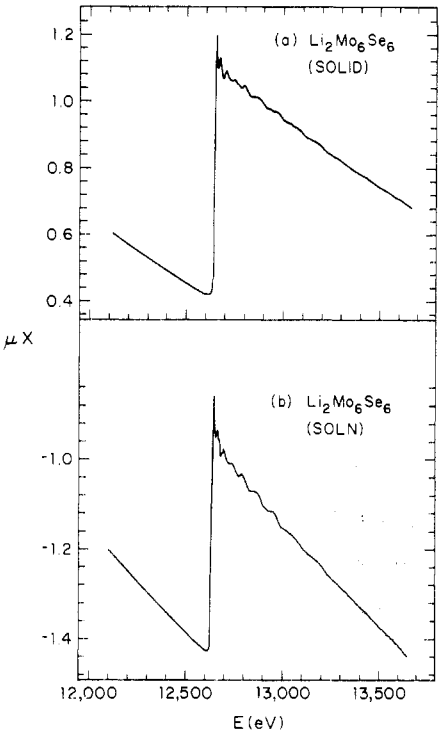

Figure 2. Se K-edge of (a) $Li_2Mo_6Se_6$ and (b) $Li_2Mo_6Se_6$/PC displayed as ln (A/A_0) vs. E in eV.

data sets extending 860 eV above the K edge of Mo and Se. Before background removal, the X-ray photon energy was converted to the photoelectron wave vector **k** ($\mathbf{k} = [2m/\hbar^2(E - E_0)]^{1/2}$, where m is the mass of the electron and E_0 is the observed K-edge energy), and the data were weighted by a factor of $\mathbf{k}^3$ to offset attenuation of the EXAFS signal with increasing photon energy. The background was removed by use of a five-section cubic spline ($\Delta\mathbf{k}$ = ca. 2.97 Å^{-1}/section). The EXAFS signal ($\mathbf{k}^3[\chi(\mathbf{k})]$ vs. **k**) was normalized by dividing by the edge jump and corrected for absorption dropoff by means of Victoreen's true absorption coefficients.[9] The background-removed data were truncated at 3 and 15 Å^{-1} before Fourier transformation.

Following Fourier transformation, the resultant peaks were isolated and filtered by use of a window function centered on the peaks. After filtering, the isolated peaks were back transformed to **k** space and truncated once more on each end of the data set (at 4 and 14 Å^{-1}), to minimize truncation noise generated by Fourier transformation of the finite data sets. The individually filtered data were then fitted with the single-electron single-scattering EXAFS equation (except the fourth peak of the Se spectra (vide infra))

$$\mathbf{k}^3[\chi(\mathbf{k})] = \sum_{n=1}^{m} B_n[F_n(\mathbf{k})]\mathbf{k}^2 e^{-2\sigma_n^2\mathbf{k}^2} \sin [2\mathbf{k}r_n + \Phi_n(\mathbf{k})]/r_n^2$$

where B_n, $F_n(\mathbf{k})$, $\Phi_n(\mathbf{k})$, σ_n, r_n, and **k** denote a scaling factor proportional to the number of backscatterers present, amplitude, phase, Debye–Waller factor, interatomic distance, and photoelectron wave vector, respectively, for backscattering pair n in a peak fit with m terms. Theoretical amplitude and phase functions calculated by Teo and Lee[7] were used in the curve-fitting procedure, during which four terms were optimized for each component of the peak: B_n, σ_n, r_n, and ΔE_n, the difference between the experimentally observed and theoretical K-edge energy. The theoretical phase functions are defined for an E_0 value determined from an atomic model that is not related to the actual molecular environment of the backscattering pair; therefore, ΔE_n was adjusted during the peak-fitting procedure. Interatomic backscattering distances derived from best fit based on theory (BFBT) results are listed in Tables I and II.

To improve the accuracy of the EXAFS analysis, a fine adjustment based on model compound (FABM) procedure[8] was applied, using $Tl_2Mo_6Se_6$ as the model compound. $Tl_2Mo_6Se_6$ is isomorphous to $Li_2Mo_6Se_6$, and its structure has been established by X-ray crystallography.[3a] In the FABM approach, a series of restricted fits is obtained by varying the BFBT r_n value in 0.01-Å increments and calculating a resultant ΔE_n, while holding r_n and the remaining parameters for any other peak components constant, except the scale factors B_n. The difference between the BFBT and crystallographic distance, Δr_n, for the model compound is determined, and from a plot of Δr_n vs. ΔE_n a "characteristic" ΔE_n (ΔE_n^*) is determined. This is used to fine-tune the adjustment of

Table I. Mo K-Edge EXAFS Results

	pk I		pk II	pk III	
	Mo–Mo	Mo–Se	Mo–Mo	Mo–Mo	Mo–Se
		r(BFBT)[a]			
$Tl_2Mo_6Se_6$	2.707	2.771	3.823	4.484	4.592
$In_2Mo_6Se_6$	2.712	2.779	3.837	4.476	4.576
$Li_2Mo_6Se_6$	2.712	2.791	3.834	4.472	4.574
$Li_2Mo_6Se_6$/PC	2.728	2.806	3.835	4.482	4.566
		r(FABM)[b]			
$Tl_2Mo_6Se_6$	2.697	2.650	3.802	4.478	4.575
$In_2Mo_6Se_6$	2.693	2.620	3.801	4.471	4.568
$Li_2Mo_6Se_6$	2.689	2.636	3.799	4.461	4.565
$Li_2Mo_6Se_6$/PC	2.696	2.612	3.802	4.463	4.560
		Coordination Number[c]			
$Tl_2Mo_6Se_6$	6.6	5.8	2.0	1.7	6.0
$In_2Mo_6Se_6$	5.9	4.4	1.9	1.7	6.0
$Li_2Mo_6Se_6$	6.0	4.0	2.0	2.0	6.0
$Li_2Mo_6Se_6$/PC	6.4	3.4	2.0	2.3	6.0
σ^{*}[d]	0.0397	0.0826	0.0422	0.0396	0.0819
ΔE^{*}[e]	−15.00	−17.60	−5.67	−13.67	−2.79

[a] Best fit based on theory (BFBT) average interatomic distances in Å. See text for details. [b] Fine adjustment based on model compound (FABM) average interatomic distances in Å. See text for details. [c] Number of backscatters at calculated average distances contributing to the term determined from the fine-tuning procedure using $Li_2Mo_6Se_6$ as a model compound.[8] [d] Characteristic Debye–Waller parameter determined from a model compound ($Li_2Mo_6Se_6$) and used in fine-tuning of coordination numbers.[8] [e] Characteristic ΔE (difference between calculated and observed K-edge energy during curve fitting) in eV, determined from a model compound ($Tl_2Mo_6Se_6$) during fine-tuning of interatomic distances.[8]

(7) Teo, B. K.; Lee, P. A. *J. Am. Chem. Soc.* **1979**, *101*, 2815.
(8) Teo, B. K.; Antonio, M. R.; Averill, B. A. *J. Am. Chem. Soc.* **1983**, *105*, 3751.
(9) *International Tables for X-Ray Crystallography*; Macgillavry, C. H., Rieck, G. D., Lonsdale, K., Eds.; Kynoch: Birmingham, England, 1968; Vol. III, pp 171–173.

Table II. Se K-Edge EXAFS Results

	pk I	pk II	pk III		pk IV	
	Se–Mo	Se–Se	Se–Se	Se–Mo	Se–Se	Se–Mo
			r(BFBT)[a]			
$Tl_2Mo_6Se_6$	2.632	3.796	4.500	4.541	5.240	5.070
$In_2Mo_6Se_6$	2.629	3.770	4.488	4.533	5.251	5.048
$Li_2Mo_6Se_6$	2.628	3.797	4.509	4.552	5.233	5.046
$Li_2Mo_6Se_6$/PC	2.611	3.762	4.508	4.560	5.224	5.036
			r(FABM)[b]			
$Tl_2Mo_6Se_6$	2.650	3.795	4.446	4.575	5.230	5.180
$In_2Mo_6Se_6$	2.642	3.762	4.435	4.568	5.214	5.165
$Li_2Mo_6Se_6$	2.633	3.742	4.441	4.594	5.205	5.163
$Li_2Mo_6Se_6$/PC	2.624	3.738	4.448	4.614	5.233	5.166
			Coordination Number[c]			
$Tl_2Mo_6Se_6$	2.7	4.2	2.4	4.0	1.3	1.6
$In_2Mo_6Se_6$	3.4	5.6	3.6	6.2	2.5	2.6
$Li_2Mo_6Se_6$	4.0	6.0	4.0	6.0	2.0	2.0
$Li_2Mo_6Se_6$/PC	5.1	7.8	4.3	6.2	1.7	2.0
σ^{*}[d]	0.0652	0.0792	0.0329	0.0002	0.0924	0.0538
ΔE^{*}[e]	−0.60	6.20	13.58	24.58	−6.60	24.80

[a] Best fit based on theory (BFBT) average interatomic distances in Å. See text for details. [b] Fine adjustment based on model compound (FABM) average interatomic distances in Å. See text for details. [c] Number of backscatters at calculated averaged distances contributing to the term determined from the fine-tuning procedure using $Li_2Mo_6Se_6$ as a model compound.[8] [d] Characteristic Debye–Waller parameter determined from a model compound ($Li_2Mo_6Se_6$) and used in fine-tuning of coordination numbers.[8] [e] Characteristic ΔE (difference between calculated and observed K-edge energy during curve fitting) in eV, determined from a model compound ($Tl_2Mo_6Se_6$) during fine-tuning of interatomic distances.[8]

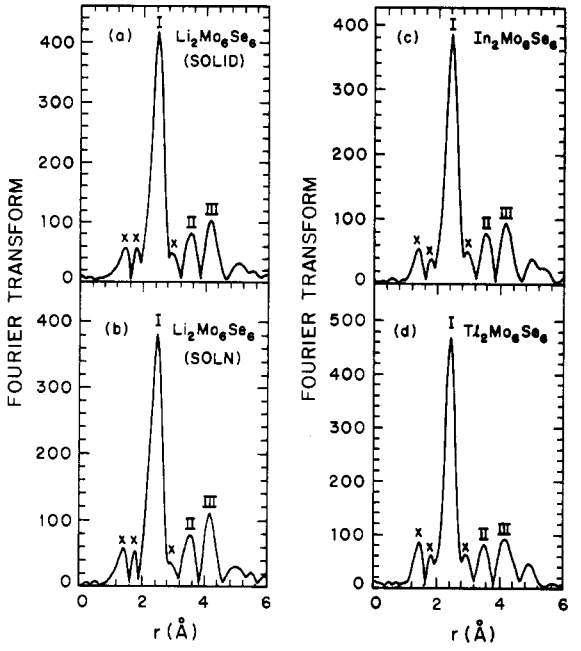

Figure 3. Fourier transforms of Mo edge EXAFS of (a) $Li_2Mo_6Se_6$, (b) $Li_2Mo_6Se_6$/PC, (c) $In_2Mo_6Se_6$, and (d) $Tl_2Mo_6Se_6$. Peaks discussed in the text are identified with Roman numerals; extraneous peaks are marked with an ×.

the theoretical E_0 value to the real world. The Δr_n for each unknown at ΔE_n^* is then determined from a Δr_n vs. ΔE_n plot and applied to the BFBT values to derive the FABM values. The procedure is repeated for σ_n and B_n, where the value of σ_n is varied in 0.005-Å increments, and a characteristic σ_n (σ_n^*) is derived, from which FABM B_n values and, hence, coordination numbers are obtained. Because of the lack of detailed knowledge of the vibrational behavior of the backscattering atom pairs, the σ_n value determined for the model compound was accepted as σ_n^*. In addition to improving the accuracy of the fitted structural parameters, the FABM procedure provides a means of checking the appropriateness of the model compounds, as well as alleviating (to some extent) the problem of parameter correlation. The FABM results, including ΔE_n^* and σ_n^* values, are presented in Tables I and II.

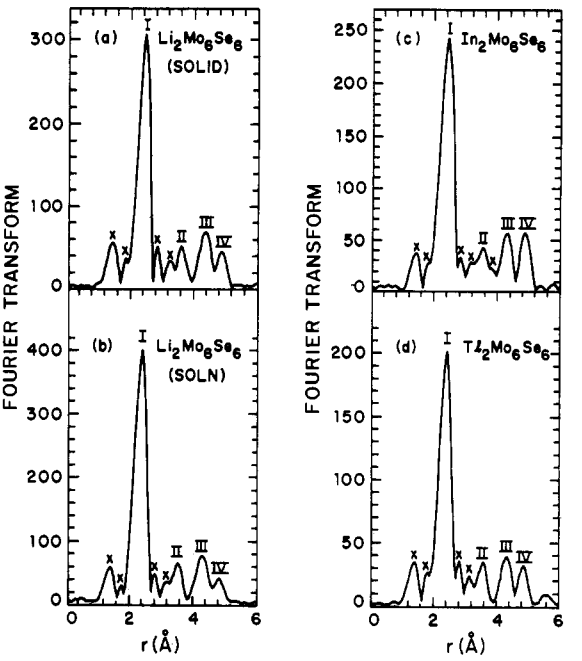

Figure 4. Fourier transforms of Se edge EXAFS of (a) $Li_2Mo_6Se_6$, (b) $Li_2Mo_6Se_6$/PC, (c) $In_2Mo_6Se_6$, and (d) $Tl_2Mo_6Se_6$. Peaks discussed in the text are identified with Roman numerals; extraneous peaks are marked with an ×.

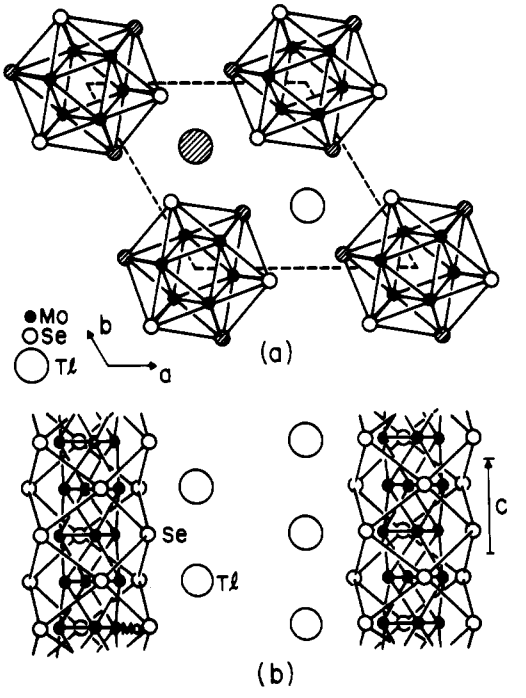

Figure 5. Structure of $Tl_2Mo_6Se_6$.[3a] Hatched atoms are at 0.25 unit and open atoms are at −0.25 unit along c_H.

Results and Discussion

Fourier transformations of the Mo and Se EXAFS yield very similar spectra for all compounds. The Mo EXAFS spectra exhibit three coordination shells (Figure 3), with an intense peak at r' = 2.4 Å and two smaller peaks at r' = 3.5 and 4.2 Å (r' = distance uncorrected for phase shift). The width of the base of the windows used for peaks I, II, and III of the Mo edge was 1.4, 1.0, and 0.9 Å, respectively. The Se EXAFS spectra (Figure 4) are characterized by an intense peak at r' = 2.3 Å and three smaller peaks at r' = 3.5, 4.3, and 4.9 Å. The Se edge peaks were isolated and filtered by the use of windows that were 1.5, 0.8, 0.9, and 0.9 Å wide at the base for peaks I, II, III, and IV, respectively.

Table III. $Tl_2Mo_6Se_6$ Crystallographic Data[a] Calculated from Ref 3a

	Mo–Mo		Mo–Se or Se–Mo		Se–Se	
peak[b]	$r \times n$[c]	av	$r \times n$[c]	av	$r \times n$[c]	av
I	2.661 × 2		2.609 × 1			
	2.715 × 4	2.697	2.619 × 1	2.65		
			2.685 × 2			
II	3.802 × 2	3.802			3.758 × 4	
					3.869 × 2[d]	3.795
III			4.510 × 1[d]			
	4.478 × 2	4.478	4.555 × 1	4.575	4.414 × 2[d]	4.446
			4.593 × 2		4.478 × 2	
			4.599 × 2			
IV			5.183 × 2	5.183	5.230 × 2	5.23

Mo–Tl: 3.756 × 1, 4.665 × 2.
Se–Tl: 3.392 × 2, 3.433 × 1; av 3.406

[a] Interatomic distances are in Å. [b] Coordination shells are labeled by the EXAFS peaks to which they contribute. [c] Number of atoms at stated distance. [d] Interchain pair.

The model compound, $Tl_2Mo_6Se_6$, is composed of parallel $(Mo_3Se_3^-)_\infty^1$ chains, between which the thallium atoms are located as illustrated in Figure 5. Conceptually, the $(Mo_3Se_3^-)_\infty^1$ chains are formed from the discrete Mo_6Se_8 clusters found in the better known Chevrel phases by removal of the face-capping Se atoms on two opposite faces of the Mo_6 octahedra and fusing the exposed Mo_3Se_3 triangular faces. Repetition of this condensation process generates the $(Mo_3Se_3^-)_\infty^1$ chains that form the $A_2Mo_6Se_6$ phases (A = +1 cation). From the X-ray crystallographic data on $Tl_2Mo_6Se_6$, all atoms within a 6-Å radius of a Mo atom or a Se atom were identified to determine the composition and distances of the coordination shells around the atoms. The results are presented in Table III.

The Mo and Se EXAFS of the solid and solution samples of $Li_2Mo_6Se_6$ are strikingly similar. No new peaks in the EXAFS of $Li_2Mo_6Se_6$/PC are observed due to solvent coordination to $(Mo_3Se_3^-)_\infty^1$ strands; conversely, no peaks present in the EXAFS of $Li_2Mo_6Se_6$ disappear in the EXAFS of the solution samples. Inspection of the X-ray structure of $Tl_2Mo_6Se_6$ (Table III) reveals that Mo has only one interchain scattering partner at a distance less than 5 Å, while Se is involved in five interchain scattering interactions. The Se EXAFS is therefore expected to be most sensitive to any change in the environment of the $(Mo_3Se_3^-)_\infty^1$ strands. As $Li_2Mo_6Se_6$ dissolves, solvent should separate the $(Mo_3Se_3^-)_\infty^1$ strands, weakening any interchain scattering interactions, if these can be detected in the Se EXAFS spectrum.

The spectra exhibit a relatively large number of coordination shells at relatively long distances in comparison with the EXAFS spectra of other compounds. A distance of 5 Å is usually the maximum observed in EXAFS due to damping and scattering of the photoelectrons responsible for the EXAFS phenomenon. A Se–Se interaction at 5.23 Å is clearly observed in the Se edge EXAFS, due to enhancement by the focusing effect[10,11] along a 179.8° Se–Mo–Se angle within the cluster chains. An unenhanced Mo–Se backscattering event is present at 5.18 Å, but its contribution to the peak is minimal, as illustrated by the fact that the corresponding Mo–Se interaction is only weakly observed above the background noise in the Mo edge EXAFS. The focusing effect is the enhanced forward scattering of photoelectrons by an intermediary atom (in this case, Mo) that occurs when the absorbing, intermediary, and backscattering atoms form an angle of 150° or larger. The intermediary atom introduces an additional amplitude and phase component to the EXAFS signal that depends on the bond angle of the nearly collinear array. Application of modified phase and amplitude functions as described by Teo[10] allowed the Se···Se distance to be calculated.

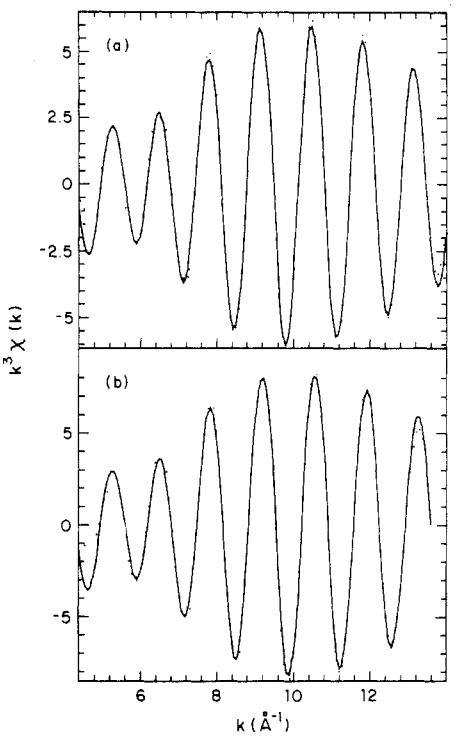

Figure 6. Filtered data (dotted curve) and best-fit result of theoretical curve fitting (solid curve) for peak I of the Mo edge of (a) $Li_2Mo_6Se_6$ and (b) $Li_2Mo_6Se_6$/PC.

Another feature of the EXAFS spectra is the absence of Mo–cation or Se–cation backscattering interactions. None of the peaks fitted required a Mo– or Se–cation term, and no peaks could be identified as arising from a Mo– or Se–cation interaction. These interactions appear to be too weak to be isolated from background noise, even though the Mo– and Se–cation distances from Table I are 3.756 and 3.406 Å, respectively, for $Tl_2Mo_6Se_6$. The atom–cation backscattering may be weak because the cation is not directly bonded to either Mo or Se, and the cations appear to be disordered around their crystallographic positions. The Tl thermal parameters in the X-ray structure study of $Tl_2Mo_6Se_6$ are much larger than those for Mo or Se.[3a] The resultant disorder in the coordination shell composed of cations thus generates only a weak backscattering interaction.

The Mo K-edge EXAFS spectra were fit by using five backscattering pairs. Peaks I and III were each fit with both Mo–Mo and Mo–Se backscattering pairs, while peak II was fit with a Mo–Mo interaction. In Figure 6, the filtered data for peak I as well as the BFBT results are shown for the two $Li_2Mo_6Se_6$ phases. Figure 7 shows the background-removed EXAFS signal ($\mathbf{k}^3[\chi(\mathbf{k})]$) and the summed BFBT results for all three peaks. Inspection of Figure 7 shows that all major features of the spectra have been fairly well reproduced. The BFBT distances for the model compound ($Tl_2Mo_6Se_6$) were, with one exception, within 0.02 Å (error <1%) of the average distance for each type of backscatterer calculated from the X-ray crystallographic data. Examination of the FABM distances shows them to be clustered around similar values. An estimate of the error in the FABM distances calculated can be made by comparing the Mo–Mo term in peak III, which is essentially the height of a unit cell, to c_H, the hexagonal cell parameter determined by powder X-ray diffraction for $Tl_2Mo_6Se_6$

(10) Teo, B. K. *J. Am. Chem. Soc.* **1981**, *103*, 3990. The modified EXAFS equation used is

$$\mathbf{k}^3[\chi(\mathbf{k})] = B_{AC}[\Omega_B(\beta,\mathbf{k})][F_{AC}(\mathbf{k})]\mathbf{k}^2 e^{-2\sigma_{AC}^2\mathbf{k}^2} e^{-2\eta\sigma_{AC}/k_{AC}} \times \frac{\sin[2\mathbf{k}r_{AC} + \Phi_{AC}(\mathbf{k}) + \omega_B(\beta,\mathbf{k})]}{r_{AC}^2}$$

where β, $\Omega(\beta,\mathbf{k})$, and $\omega(\beta,\mathbf{k})$ are defined according to eq 8, 21, and 22 in the reference and the terminal atoms, A and C, of the nearly linear array are Se and the intermediary atom, B, is Mo. For these compounds, β and r_{AC} used in calculating $\Omega(\beta,\mathbf{k})$ and $\omega(\beta,\mathbf{k})$ were obtained from the crystallographic data for $Tl_2Mo_6Se_6$; $\theta_{Mo}(\beta,\mathbf{k})$ and $F_{Mo}(\beta,\mathbf{k})$ values were calculated by Teo. Following calculation of $[\Omega_B(\beta,\mathbf{k})][F_{AC}(\mathbf{k})]$ and $\Phi_{AC}(\mathbf{k}) + \omega_B(\beta,\mathbf{k})$, the EXAFS analysis continued in the same manner as for the other terms.

(11) Lee, P. A.; Pendry, J. B. *Phys. Rev. B: Solid State* **1975**, *11*, 2795.

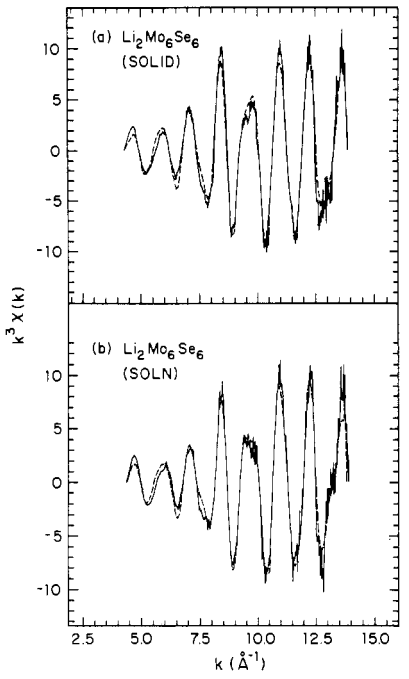

Figure 7. Background-removed EXAFS (solid curve) and summed best-fit results of theoretical curve fitting (dashed curve) for the Mo edge of (a) $Li_2Mo_6Se_6$ and (b) $Li_2Mo_6Se_6$/PC.

(4.478 Å), $In_2Mo_6Se_6$ (4.497 Å), and $Li_2Mo_6Se_6$ (4.48 Å).[12] The largest difference between the FABM and the X-ray values is 0.026 Å (~0.6%), except for one term (Table I: Mo edge, Mo–Se term of peak I). The difference in r_{FABM} between $Li_2Mo_6Se_6$ and $Li_2Mo_6Se_6$/PC is generally less than 0.01 Å, well within experimental error (ca. 1%). The difference in the Mo–Se term of peak I between the solid and solution structures of $Li_2Mo_6Se_6$ probably results from parameter correlation in the curve-fitting routine.

The Se K-edge EXAFS spectra were fit with six backscattering pairs. Peaks I and II were fit with just one term each (Se–Mo and Se–Se, respectively), while peaks III and IV were both fit with two terms each (Se–Se and Se–Mo backscatterings). Figure 8 shows the BFBT results and the filtered experimental data for peak I, and Figure 9 shows the background-removed EXAFS signal ($\mathbf{k}^3[\chi(\mathbf{k})]$) and the summed BFBT results for all the peaks analyzed. The BFBT distances for the model compound were, again with one exception, within 0.05 Å (error <1.1%) of the X-ray crystallographic distances. All fine-tuned distances are also tightly grouped around similar values. Separation of the $(Mo_3Se_3^-)_\infty^1$ strands should result in r_{FABM} shortening for peak II and lengthening for the two terms of peak III, if interchain contacts make an appreciable contribution to the EXAFS. However, $Li_2Mo_6Se_6$ and $Li_2Mo_6Se_6$/PC FABM distances show only minor variations (difference <0.6%).

The determination of the number of backscatterers from the Mo and Se edge data was based upon the best-fit results for $Li_2Mo_6Se_6$. During the fine-tuning procedure to determine coordination numbers, the Se edge of the $Tl_2Mo_6Se_6$ model compound exhibited anomalous behavior with respect to the other three compounds. The artifact is inherent in the data set analyzed and is not a problem with the FABM procedure, as the amplitude of the Fourier-transformed EXAFS of $Tl_2Mo_6Se_6$ (from analysis of which coordination numbers are obtained) is about two-thirds of that observed in the other three data sets. Consequently, $Li_2Mo_6Se_6$ was chosen as the best model compound for calculation of coordination numbers in the fine-tuning procedure. The fine-tuning of distance was performed relative to $Tl_2Mo_6Se_6$, as r is calculated through analysis of the phase of the EXAFS oscillations, not the amplitude. For consistency, the Mo edge coordination numbers were also calculated relative to $Li_2Mo_6Se_6$,

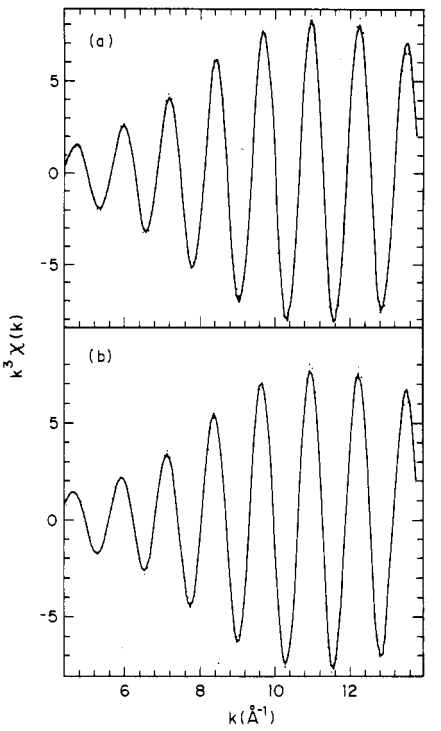

Figure 8. Filtered data (dotted curve) and best-fit result of theoretical curve fitting (solid curve) for peak I of the Se edge of (a) $Li_2Mo_6Se_6$ and (b) $Li_2Mo_6Se_6$/PC.

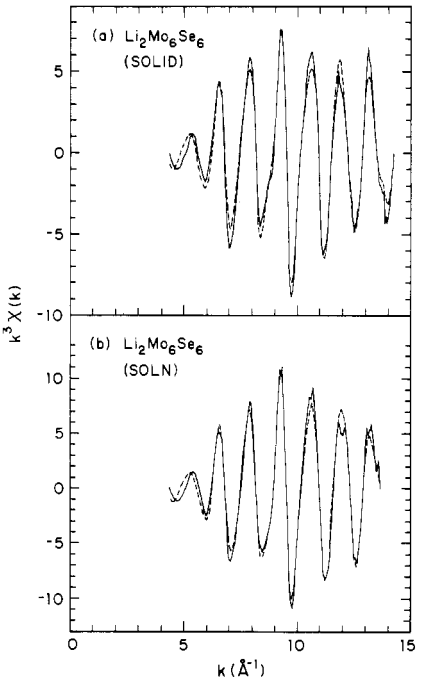

Figure 9. Background-removed EXAFS (solid curve) and summed best-fit results of theoretical curve fitting (dashed curve) for the Se edge of (a) $Li_2Mo_6Se_6$ and (b) $Li_2Mo_6Se_6$/PC.

although the $Tl_2Mo_6Se_6$ Mo K-edge data did not exhibit the same anomalous behavior. The source of the different behavior of the Se and Mo edges of the model compound is uncertain but could be a combination of thickness effect,[13] grain-size effects,[14] and the presence of a larger amount of harmonics in the incident X-ray beam at the lower Se K-edge energy vs. the Mo K-edge energy. The factors mentioned above cause the amplitude of the EXAFS

(12) Huster, J.; Schiffers, G.; Bronger, W. *J. Less-Common Met.* **1983**, *91*, 333.

(13) Heald, S. M.; Stern, E. A. *Phys. Rev. B: Solid State* **1977**, *11*, 5549. Stern, E. A.; King, K. *Phys. Rev. B: Condens. Matter* **1981**, *23*, 3781.

(14) Lu, K. Q.; Stern, E. A. *Nucl. Instrum. Methods* **1981**, *212*, 3781.

to be less than expected for the number of backscatterers present, resulting in the calculation of coordination numbers that are too low.

The coordination numbers for the Mo edge data are rather similar, showing differences of only 10–15% (except for the Mo–Se term of peak I of $Tl_2Mo_6Se_6$, which is subject to parameter correlation in the curve-fitting procedure). The calculated coordination numbers for the Se edge show substantially more variation, ca. 30%. Formation of individual $(Mo_3Se_3^-)_\infty^1$ strands should result in a decrease in the coordination numbers for peaks II and III for $Li_2Mo_6Se_6$/PC vs. $Li_2Mo_6Se_6$, if interchain contacts contribute appreciably to the EXAFS. Instead, however, a very slight increase in the coordination numbers is actually observed.

Conclusions

The lack of major differences between the EXAFS spectra of $Li_2Mo_6Se_6$ and $Li_2Mo_6Se_6$/PC indicates that the Se and Mo environments in the samples are indistinguishable. Analysis of the Mo and Se EXAFS shows that both are dominated by *intra*chain scattering interactions; consequently, the structure of the $(Mo_3Se_3^-)_\infty^1$ chain is not observed to be perturbed significantly upon dissolution. *Inter*chain interactions make only a relatively minor contribution to the Se and Mo EXAFS, and no significant changes attributable to these contacts were observed. These results are consistent with previous TEM studies, which have demonstrated that $Li_2Mo_6Se_6$ in propylene carbonate forms bundles of one-dimensional chains whose diameter decreases with increasing dilution. Within the concentration range amenable to study by EXAFS spectroscopy, these bundles are of sufficiently large diameter (≥20 Å) that the bulk of the material lies in the interior of the bundle in an environment very similar to that of the crystalline phase. The fraction of the material on the surface of the bundle and in direct contact with the solvent is small and does not make an observable contribution to the EXAFS. Despite the complexity of the system and the presence of multiple contributions to the EXAFS, analysis of the data yielded average bond distances in good agreement with X-ray results for $Tl_2Mo_6Se_6$.

Acknowledgment. This research was supported in part by the National Science Foundation—Solid State Chemistry—Grant DMR-8313252 (D.A.H. and B.A.A.). We thank the staff at CHESS and S. M. Kauzlarich for their assistance and the following people for their help in collecting the data: M. R. Antonio, S. Burman, W. Frazier, O. Fussa, C. L. Hulse, J. Orlando, and T. Zirino.

Registry No. $Li_2Mo_6Se_6$, 92341-41-8; $In_2Mo_6Se_6$, 75036-77-0; $Tl_2Mo_6Se_6$, 73667-07-9; Mo, 7439-98-7; Se, 7782-49-2; propylene carbonate, 108-32-7.

Supplementary Material Available: Figures of background-removed EXAFS ($\mathbf{k}^3[\chi(\mathbf{k})]$ vs. $\mathbf{k}$) from Mo and Se edges of $Li_2Mo_6Se_6$, $Li_2Mo_6Se_6$/PC, $In_2Mo_6Se_6$, and $Tl_2Mo_6Se_6$ and tables of parameters (r, ΔE, σ, B) determined from curve fitting of the theoretical EXAFS equation to filtered data of Mo and Se edge EXAFS (11 pages). Ordering information is given on any current masthead page.

Contribution No. 7439 from The Chemical Laboratories, California Institute of Technology, Pasadena, California 91125

A Novel Nonplanar Amido-*N* Ligand Type. Nonplanarity in the Amido-*N* Ligand Induced by Steric Effects

Terrence J. Collins,*[1] Ting Lai, and Geoffrey T. Peake

Received November 19, 1986

The X-ray crystal structure of Os(η^3-(H)HBA-B)(PPh_3)(phen) (**2**; the free-base ligand is H_4HBA-B = 1,2-bis(2-hydroxybenzamido)benzene; phen = 1,10-phenanthroline), an osmium(III) complex containing a tridentate phenolato–diamido-*N* ligand, is reported. Crystal data: $OsC_{50}H_{35}N_4O_4P\cdot 2C_2H_5OH$, a = 10.448 (4) Å, b = 14.454 (6) Å, c = 16.598 (7) Å, α = 89.27 (3)°,

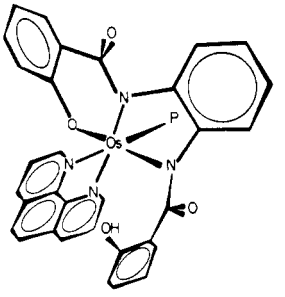

2

β = 99.74 (3)°, γ = 111.44 (3)°, V = 2296 (1) Å^3, triclinic, $P\bar{1}$, Z = 2, $R(I > 0)$ = 0.054 (7897 reflections), $R(I > 3\sigma(I))$ = 0.047 (6986 reflections). This molecule contains the first member of a new class of nonplanar amido-*N* ligands where the nonplanarity can be attributed to steric effects. The amido-*N* ligand with the uncoordinated hydroxybenzoyl arm is distinctly nonplanar with a $\bar{\tau}$ value (a twist angle about the C–N bond) of −40°. The χ_N value (an angle reflecting pyramidal distortion at N) of −49° is the largest for any organic amido-*N* ligand, and the χ_C value of −10° is as large as any that have been observed previously.

Introduction

We have recently reported the first cases of nonplanar organic amido-*N* ligands with large twist angles about the C–N bond.[2] The twisting can be quantified by the angle $\bar{\tau}$, which approximates the smaller angle between the carbonyl carbon and the nitrogen parent pπ orbitals (Figure 1).[2] Of the 120 structurally characterized cases of monodentate metallo–amido-*N* groups derived from parent mono-N-substituted amides, only nine have $\bar{\tau}$ values greater than 10°. The known cases are confined to complexes of polyanionic chelating (PAC) ligands of the type described here. Two distinct classes of complexes of nonplanar amido-*N* ligands, distinguished by the nature of the primary cause of the nonplanarity, have already been identified: (i) in class I complexes, nonplanar amido-*N* ligands are formed because nonplanar amido-*N* ligands are thermodynamically favored over planar analogues

(1) Alfred P. Sloan Research Fellow, 1986–1988; Dreyfus Teacher-Scholar, 1986–1990.
(2) Collins, T. J.; Coots, R. J.; Furutani, T. T.; Keech, J. T.; Peake, G. T.; Santarsiero, B. D. *J. Am. Chem. Soc.* **1986**, *108*, 5333–5339.

0020-1669/87/1326-1674$01.50/0